Detection, damping, and translating the center of the axial oscillation of a charged particle in a Penning trap with hyperbolic electrodes

Gerald Gabrielse
Department of Physics, FM-15, University of Washington, Seattle, Washington 98195
(Received 22 June 1983)

The axial oscillation frequency of a trapped particle in a Penning trap with hyperbolic electrodes has proven to be a very important observable for precision experiments. Shifts in this frequency have been used to measure magnetron frequencies, cyclotron frequencies, and $g-2$ transitions for single trapped particles. Detection and damping of the axial oscillation were thought to be well understood except that a key constant which depends upon trap geometry had not been calculated. A relaxation calculation has thus been performed to provide a calculated value for this constant and several others, and to determine their dependence upon trap geometry. A surprising result is a discrepancy between the calculated value of the key constant and that deduced from measured values of the width of the axial oscillation frequency in the several cases where it has been measured.

I. INTRODUCTION

A single electron was first trapped in a Penning trap ten years ago.[1] Subsequent progress[2] led to measurements of the magnetic moments of both the electron[3] and positron[4] to accuracies of 5×10^{-11}. The measurement of the magnetic-moment anomalies are the most stringent tests of quantum electrodynamics, which has been used to calculate the anomalies to order α^4 (in Ref. 5). Comparison of the electron and positron magnetic moment provides a rigorous test of the invariance of the electron-positron system under CPT (combined charge-conjugation, parity, and time-reversal transformations.). An experiment now underway, whose ultimate goals include trapping a single proton, has already produced the most accurate ratio of the electron and proton masses.[6] Another experiment is underway with a goal of improving the accuracy of the measured magnetic moments of the electron to 10^{-12} or better.[7] The frequency of the axial oscillation (along magnetic field lines) is a crucial observable in all of these experiments. Small shifts in this frequency are used to detect magnetron frequencies, cyclotron frequencies, and $g-2$ transitions.

An earlier paper discussed a relaxation calculation of the static trapping and compensation potentials in Penning traps with hyperbolic endcap and ring electrodes.[8] An orthogonalized configuration of hyperbolic trap electrodes was proposed to make the harmonic-oscillation frequency of a trapped particle to be independent of adjustments in the compensation potential. The compensation potential is applied to additional electrodes in order to tune out trap anharmonicities. In this paper, these static quadrupole trapping potentials are not discussed. The focus is instead upon additional potentials superimposed upon the electrodes because of, and to modify, the axial motion of a trapped particle. These include static potentials to move the center of the axial oscillation, oscillatory potentials on the electrodes which drive the axial motion, and potentials induced on the electrodes by this axial motion. For a particular configuration of trap electrodes, all of these are manifestations of only one electrostatic solution to Laplace's equation, identified as ϕ_A in Sec. II.

Similar techniques are employed to calculate ϕ_A as a function of electrode geometry as were employed to calculate the static trapping potentials within compensated Penning traps.[8] These are discussed in Sec. III. The same transformation of coordinates is used to avoid mismodeling hyperbolic electrodes. A crucial difference is that ϕ_A is odd under the reflection $z\rightarrow-z$ whereas the previously calculated solutions are even. The resulting incompatibility of ϕ_A and the intrinsically even coordinates is remedied by solving for an even function χ (by relaxation) with χ defined so that $\phi_A=z\chi$. Details of the relaxation calculation covered in the earlier paper[8] are not repeated. The solution ϕ_A turns out to be particularly simple, especially for asymptotically symmetric traps where two expansion coefficients suffice to characterize the potential over the whole possible trapping volume. The calculated value of the first of these expansion coefficients is substantially higher than a previous rough estimate.[9]

Finally, the consequences of the relaxation calculation for particle trapping are briefly discussed (in Sec. IV). Static potentials which translate the center of the axial oscillation seem to be well understood. Translating the center of the axial oscillation has proven to be useful in experiments which make use of "magnetic bottles"—to measure the size of the magnetic bottle, to determine its precise location with respect to the electric center of the trap, and finally to shift the electric center to coincide with the magnetic center.[10] Until this calculation, the accuracy in the measurement of the size of a magnetic bottle was limited because the value for a key constant, called B_1 here, was not well known. In response to this work, some earlier data for a trapped electron has since been interpreted as a measurement of B_1 and this single available measurement agrees within the measurement accuracy with the value from the relaxation calculation.[11] This measurement can only be done in a trap with a magnetic bottle

and requires the observation of the axial frequency shift which results from a spin flip[3] and, thus, is not a generally available technique.

The radio-frequency consequences of the relaxation calculation seem to be less well understood. Section IV contains a brief discussion of the damping of the axial oscillation which initially parallels the earlier work by Wineland and Dehmelt.[9] Near the center of the trap, where particles are trapped, ϕ_A is essentially approximated by its lowest-order spatially uniform electric field term. A problem is that such a lowest-order approximation of ϕ_A, with the coefficient determined by the relaxation calculation, predicts an axial resonance width which is wider than the measured widths by more than a factor of 2. This problem is not resolved by the much better two term expansion of ϕ_A suggested by the relaxation calculation, unless the average value of the magnetron radius is much larger than it has been measured to be. Efforts are now underway to understand the discrepancy.

II. ELECTROSTATICS

Figure 1 is a scale drawing of a compensated Penning trap with hyperbolic endcap and ring electrodes. Figure 2 shows the trap model used for numerical computations. The ring and endcap electrodes lie along hyperbolas identified by ρ_0 and z_0, the minimum radial and axial distances to these electrodes. Compensation electrodes are located on the quadrupole asymptote (given by $z^2=\rho^2/2$) at distance r_c from the center of the trap. They are symmetric about the asymptote and have internal angle α. All

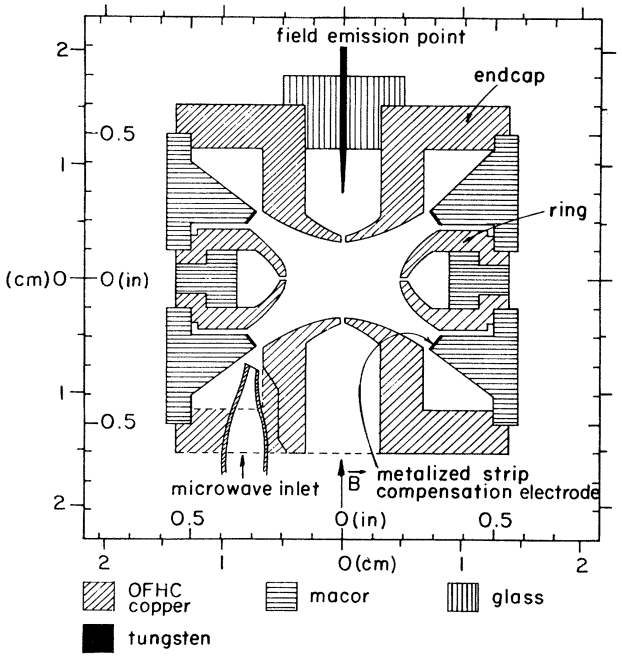

FIG. 1. Drawing of the most recently constructed compensated Penning trap. It was designed by the author and is presently being used in an attempt to measure an electron's magnetic moment to an accuracy of 10^{-12}. The drawing is to scale except for the holes in the endcap and the slit in the ring which are slightly enlarged to make them visible. The electrodes are axially symmetric about the magnetic field vector shown.

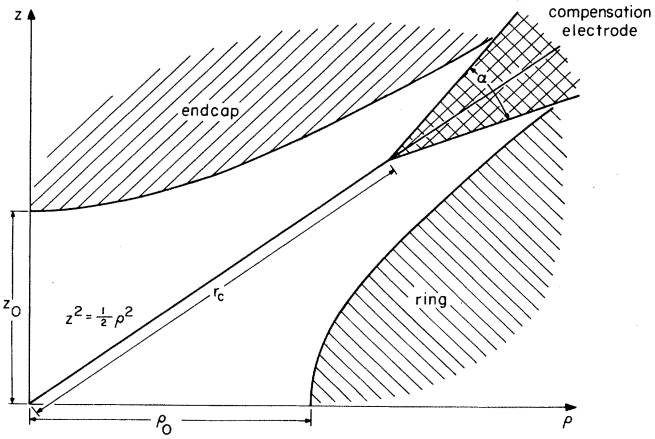

FIG. 2. Model used for a hyperbolic Penning trap. Relaxation calculations are carried out for various α and r_c as well as for various ratios of ρ_0 to z_0. The particular example shown is for an asymptotically symmetric trap with $\alpha=30°$ and $r_c/z_0\approx 2.2$.

of the electrodes are invariant under rotations about the z axis and invariant under reflections across the x-y plane. Gaps between electrodes are taken to be negligibly small.

The static quadrupole trapping potential and the static compensation potential, which are calculated and discussed in the earlier paper,[8] cause a trapped particle to oscillate harmonically along the z axis with axial oscillation frequency ω_z. Here we ignore these potentials and instead focus upon the additional potentials which are superimposed upon them. Consider first the addition of the small static potentials $V_{dc}/2$ to the upper endcap and $-V_{dc}/2$ to the lower endcap, with no additions to the ring and compensation electrodes. The offset V_{dc} could be due to imperfections in the trap or could be applied deliberately and produces a potential within the trap given by

$$V=V_{dc}\phi_A\ , \tag{2.1}$$

where ϕ_A is a solution to Laplace's equation which is antisymmetric under the reflection $z\rightarrow -z$ and which satisfies the boundary conditions in Fig. 3. To understand the consequences of the offset potential V_{dc} for particle trapping, complete knowledge of ϕ_A is not generally required because particles are typically trapped near the center of

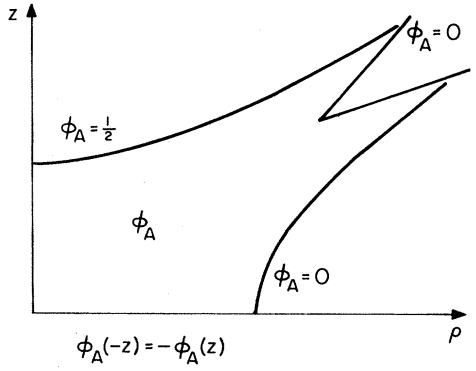

FIG. 3. Boundary conditions which uniquely define a solution to Laplace's equation ϕ_A, which is also antisymmetric under reflections across the x-y plane.

the trap. In this region [at position (r,θ,ϕ) in spherical coordinates, with $r \ll z_0$] ϕ_A can be expanded in a familiar way in powers of r/z_0 multiplied by odd order Legendre polynomials $P_k(\cos\theta)$,

$$\phi_A = \tfrac{1}{2} \sum_{\substack{k=1 \\ (\text{odd})}}^{\infty} B_k \left[\frac{r}{z_0} \right]^k P_k(\cos\theta) \ . \tag{2.2}$$

Each term in this expansion is a solution to Laplace's equation and is symmetric under rotations about the z axis and antisymmetric under reflections across the x-y plane.

Near the center of the trap $\phi_A \approx B_1 z/2z_0$. This is the potential of a spatially uniform electric field, and B_1 is equal to the constant α used by Wineland and Dehmelt.[9] For parallel plate endcaps at $z = \pm z_0$ and the ring moved far back to $\rho_0 \gg z_0$, the expansion coefficient $B_1 = 1$ and all other B_k vanish. Hyperbolic endcaps are pulled back further from the center of the trap than are the imagined flat endplates. The electric field through the center of the trap is therefore reduced so that a value of $B_1 < 1$ is expected. For large enough ρ_0/z_0, the ring will not affect the electric field near the center of the trap so that the B_k will approach limiting values which are independent of this ratio. As ρ_0/z_0 is reduced, the ring will increasingly screen the field through the center of the trap so that B_1 is further reduced. Wineland and Dehmelt estimated that $B_1 \approx \frac{1}{2}$ for asymptotically symmetric traps.

The electrostatic potential ϕ_A is also the key to understanding the additional oscillatory potentials superimposed upon the electrodes as a consequence of a trapped particle's axial oscillation at frequency ω_z and upon those applied to drive this oscillation. Because ω_z is typically a radio frequency, the associated oscillatory fields have wavelength $\lambda \gg z_0$. The interior of the trap is thus in the "near field" region where the spatial distribution of the oscillatory fields is that of the electrostatic fields produced in the trap by the instantaneous potentials on the electrodes.

To identify the boundary conditions which correspond to the instantaneous potentials consider the detection configuration of Fig. 4(a).[12] The endcaps are connected with a resistor R and the other electrodes are grounded. The instantaneous sum of the potential V_I induced across R by a trapped particle's axial motion and the Nyquist thermal noise V_n from R are detected with a differential amplifier-detector with infinite impedance. In practice, of course, an inductor is placed in parallel with R in order to tune out the capacitance of the trap and the input impedance of the amplifier contributes to R. The potential within the trap at this instant is therefore equal to

$$V = (V_I + V_n)\phi_A \ , \tag{2.3}$$

where ϕ_A is again the solution to Laplace's equation with boundary conditions in Fig. 3.

The related detection configuration in Fig. 4(b) allows the additional application of an oscillatory drive potential V_D.[3] The ring and compensation electrodes are again grounded (for radio frequencies) and V_D is applied between one endcap and ground. The resistor R is connected between the other endcap and ground so that $V_I + V_n$ is

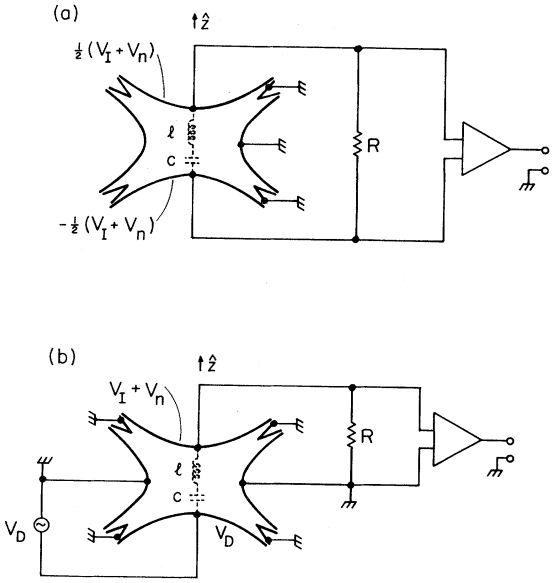

FIG. 4. Electric circuits used to detect and damp the axial resonance. The axial motion induces the potential V_I on the endcaps. The resistor R damps the axial motion and thermal noise from R produces the noise drive V_n. An external generator produces V_D. All of these potentials are oscillatory potentials.

the instantaneous potential of the other endcap. Within the trap, the potential is given by

$$V = (V_I + V_n - V_D)\phi_A + (V_I + V_n + V_D)(\tfrac{1}{4} - \tfrac{1}{4}\phi_c + \tfrac{1}{2}\phi_0) \ . \tag{2.4}$$

The first term is antisymmetric under $z \rightarrow -z$ and has the spatial distribution of ϕ_A. The second term is symmetric under $z \rightarrow -z$ and the solutions to Laplace's equation, ϕ_c

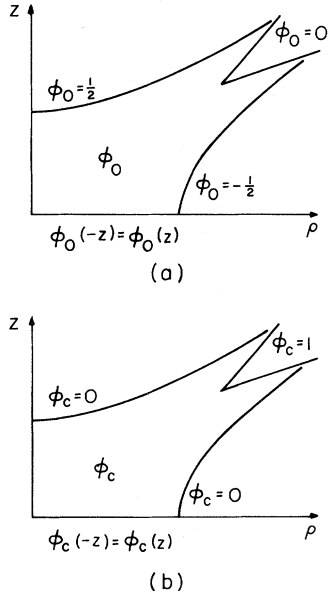

FIG. 5. Boundary conditions which uniquely define the solutions to Laplace's equation, ϕ_0 and ϕ_c, which are even under reflections across the x-y plane. These solutions were studied in Ref. 8.

and ϕ_0, are uniquely determined by their boundary conditions in Fig. 5. These solutions were calculated and discussed in Ref. 8 because of their importance for the static trapping and compensation potentials. For a good trap, ϕ_c is very small and ϕ_0 is nearly a quadrupole potential so that for our purpose here

$$\tfrac{1}{2}\phi_0-\tfrac{1}{4}\phi_c\approx\frac{z^2-\frac{1}{2}\rho^2}{2\left[z_0^2+\frac{1}{2}\rho_0^2\right]}+\text{const}\ . \tag{2.5}$$

A complete accounting of the oscillatory potentials involved in Fig. 4 thus requires only the additional calculation of ϕ_A.

III. RELAXATION CALCULATION OF ϕ_A

A relaxation calculation is used to calculate ϕ_A and hence the expansion coefficients B_k. It is basically similar to that used to calculate ϕ_c and ϕ_0 in Ref. 8 but differs in one crucial respect. Laplace's equation is again solved using the coordinates

$$s=z^2+\tfrac{1}{2}\rho^2\ , \tag{3.1}$$

$$t=z^2-\tfrac{1}{2}\rho^2 \tag{3.2}$$

so that a square mesh in (s,t) space produces mesh points exactly on the hyperbolic electrodes as shown in Fig. 6. These coordinates, however, are intrinsically even under the reflection $z\rightarrow -z$ and are thus incompatible with the odd symmetry of ϕ_A. To remedy this problem we introduce a function χ defined such that

$$\phi_A=z\chi\ . \tag{3.3}$$

More precisely, χ is defined to be equal to $1/2z$ on the upper endcap, to vanish on the ring and compensation electrodes, and to be invariant under both rotations about the z axis and the reflection $z\rightarrow -z$. In addition, χ is defined to be a solution to the differential equation

$$0=\frac{\partial^2\chi}{\partial\rho^2}+\frac{\partial^2\chi}{\partial z^2}+\frac{1}{\rho}\frac{\partial\chi}{\partial\rho}+\frac{2}{z}\frac{\partial\chi}{\partial z}\ . \tag{3.4}$$

This equation is identical to Laplace's equation in cylindrical coordinates (which ϕ_A must satisfy) except for the addition of the last term. Equation (3.4) is transformed to the coordinates s and t and solved by relaxation.

The relaxation calculation of χ and the least-squares fitting to $z\chi$ to ascertain the B_k are similar enough to that for ϕ_c and ϕ_0 in Ref. 8 that only differences are mentioned here. The relaxation formulas are slightly different because the differential equation for χ is slightly different. Convergence of χ occurs more quickly than for ϕ_c and ϕ_0 because the potential at the center of the trap does not need to penetrate through the severely screened asymptotic region. For similar reasons χ varies only slightly over the interior of the trap compared to the orders-of-magnitude variation which typically occur for ϕ_c and ϕ_0 so that a coarser mesh suffices. Figure 7 shows the calculated values of B_1, B_3, and B_5 for an asymptotically symmetric trap (defined by $\rho_0^2=2z_0^2$), with $\alpha=180°$ and $r_c/z_0=2.5$, as a function of mesh intervals in z_0. Notice that B_1 is converged within 0.2% already for ten mesh intervals, the mesh density shown in Fig. 6. Typically a mesh density of 40 intervals in z_0 was used.

The endcap and ring electrodes of the traps used for the high precision electron, positron, and proton experiments previously mentioned all lie on hyperbolas specified by $\rho_0^2=2z_0^2$. These hyperbolas are symmetric about the quadrupole asymptote ($z^2=\rho^2/2$) for large ρ and z. Figure 8 shows B_1 through B_7 for such asymptotically symmetric traps plotted as a function of the location of the compensation electrode (r_c/z_0 in Fig. 2) for variously shaped compensation electrodes (α in Fig. 2). The coefficients converge to values that are independent of both α and r_c/z_0 for $r_c/z_0>2.2$. This is the region where precision traps have been built. Notice that the calculated value of B_1 is about 60% higher than the previously estimated value[9] which is represented by the dashed line. This means that $(B_1)^2$ (which is proportional to the width of the axial resonance) is about 2.5 times greater than previously estimated. This is discussed further in Sec. IV.

The B_k in Fig. 8 are surprisingly simple. For $r_c/z_0>2.5$

$$B_1\approx 0.80\ , \tag{3.5}$$

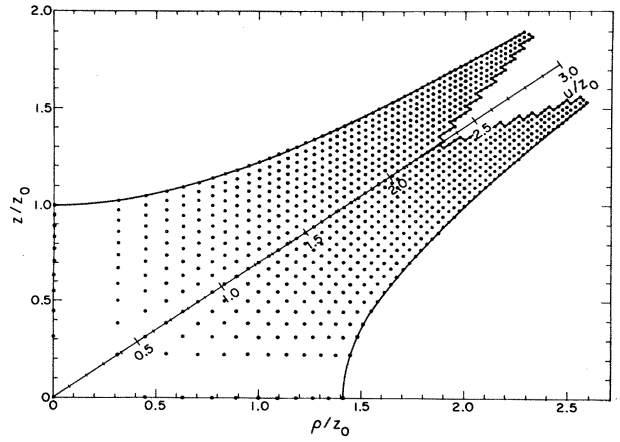

FIG. 6. Model hyperbolic trap of Fig. 2 with a square mesh in (s,t) space superimposed.

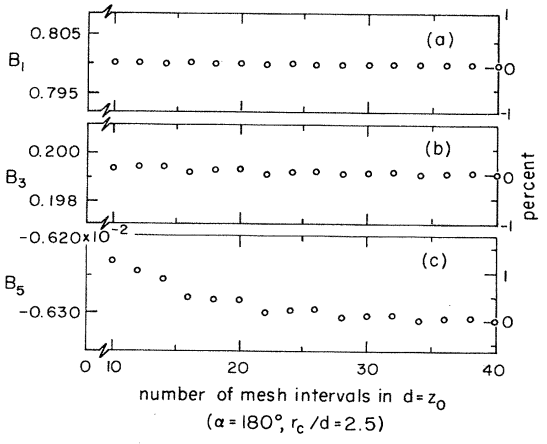

FIG. 7. Dependence of B_1, B_3, and B_5 upon the number of mesh intervals in z_0 for an asymptotically symmetric trap with $\alpha=180°$ and $r_c/z_0=2.5$.

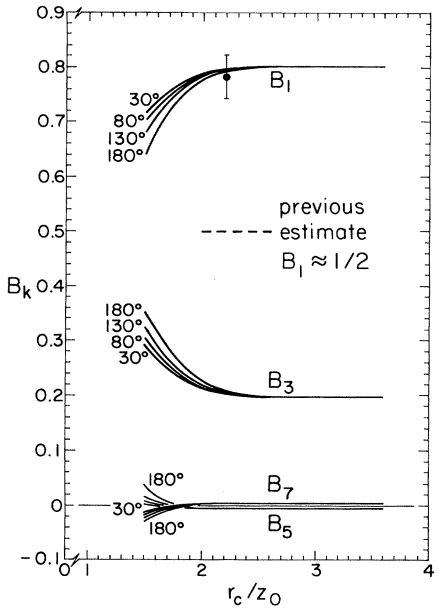

FIG. 8. B_k coefficients for asymptotically symmetric traps as a function of the location of the compensation electrode r_c/z_0 for various α. The experimental value (Ref. 11) is for a trap with $r_c/z_0=2.2$ and $\alpha=30°$.

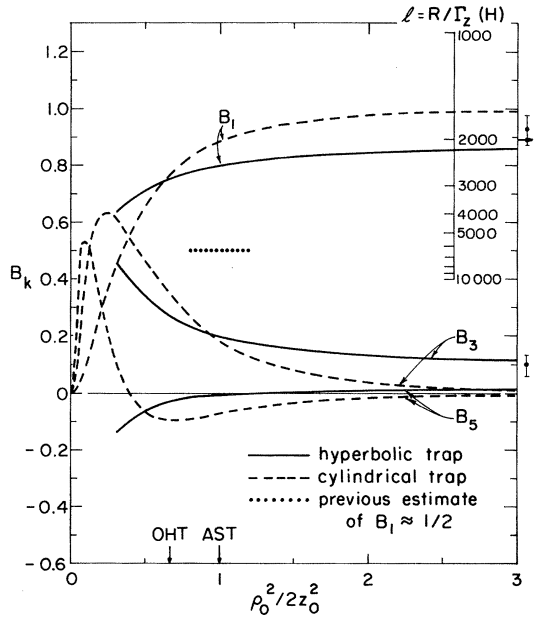

FIG. 9. B_k coefficients for hyperbolic and cylindrical Penning traps as a function of $\rho_0^2/2z_0^2$. The hyperbolic trap has $\alpha=180°$ and $r_c/d=2.5$. AST and OHT designate asymptotically symmetric trap and orthogonalized hyperbolic trap, respectively. The previous estimate of $B_1 \approx \frac{1}{2}$ is from Ref. 9. The arrow and experimental point on the right are a conformal mapping estimate and an electrolytic tank measurement (discussed in the text) which apply to the case of hyperbolic endcap electrodes and the ring moved to infinity. The additional vertical scale inserted in the upper right of the figure makes it possible to interpret the curve for B_1 directly as the effective inductance of an electron in the trap shown in Fig. 1.

$$B_3 \approx 0.20 \,. \tag{3.6}$$

For increasing r_c/z_0 it is not surprising that the B_k approach limiting values that are independent of α and r_c/z_0, because the potential in the asymptotic region is severely screened from the center of the trap by the endcap and ring electrodes. What is a pleasant surprise is that $B_1+B_3 \approx 1.00$ and that B_5 and B_7 are significantly smaller. This means that ϕ_A is described very well over the entire trapping volume $\rho<\rho_0$ (not just for $r/z_0 \ll 1$) by just the first two terms of expansion (2.2).

The solid lines of Fig. 9 show the B_k for a wide range of ρ_0/z_0. The compensation electrodes pertaining to this figure are flat ($\alpha=180°$) and are located at $r_c/d=2.5$, where d, given by

$$d^2=\tfrac{1}{2}(z_0^2+\tfrac{1}{2}\rho_0^2) \,, \tag{3.7}$$

is the characteristic trap dimension used in Ref. 8. These choices insure that the calculated B_k are essentially independent of both α and r_c/z_0 for each ρ_0/z_0. The asymptotically symmetric configuration ($\rho_0^2=2z_0^2$) and the orthogonalized configuration proposed in Ref. 8 (with $\rho_0 \approx 1.16 z_0$) are both indicated by arrows. A much wider range of $\rho_0^2/2z_0^2$ is plotted in Fig. 9 than is immediately useful for trap construction to display the limiting values of the B_k. To further clarify the qualitative features, the B_k for flat plate endcaps at $z=\pm z_0$ and a cylindrical ring at $\rho=\rho_0$ (see Fig. 10) are plotted as dashed lines. A series solution for these coefficients is readily available using standard electrostatic techniques.[13]

As expected, the B_k approach limiting values, for large $\rho_0^2/2z_0^2$, which are independent of ρ_0/z_0. For the cylindrical trap in Fig. 10, the B_k all approach zero except for B_1 which approaches 1. These are the expected limiting values for an infinite parallel plate capacitor. For the hyperbolic trap, B_1 approaches a slightly lower limiting value and B_3 approaches a limiting value somewhat greater than zero to compensate. A crude estimate for the limiting value of B_1 can be deduced from a conformal mapping solution for hyperbolic endcap electrodes (and no ring electrode) in two dimensions.[14] The electric field on the axis is reduced by 6.2% compared to the flat plate case because the two-dimensional endcap is pulled back. If we assume that the field for hyperbolic endcaps in three dimensions is approximately reduced by twice this amount, we estimate that the limiting value is $B_1 \approx 0.88$ which is very close to the calculated limit and is indicated by the arrow on the right of Fig. 9. The experimental

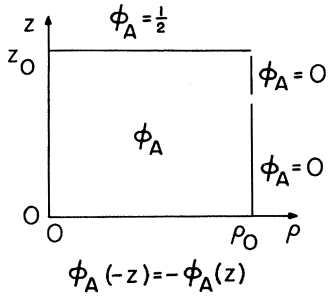

FIG. 10. Boundary conditions used in Ref. 13 to obtain the dashed curves in Fig. 9.

point on the right of Fig. 9 is a crude measurement made in an electrolytic tank for the same limit.

As $\rho_0^2/2z_0^2$ is decreased, more and more electric field lines from the endcap terminate on the ring instead of penetrating through the center of the trap and terminating on the other endcap. Thus, B_1 decreases and both B_3 and B_5 increase in magnitude to compensate. These changes are much less severe for the hyperbolic trap because the hyperbolic ring screens less severely than does the cylindrical ring. In the limit of $\rho_0^2/2z_0^2 \to 0$ the B_k are more difficult to evaluate for the hyperbolic electrodes and are not included in Fig. 9. The B_k for the cylindrical trap of Fig. 10, however, clearly show the onset of exponential screening in that B_3 and B_5 turn around and drop rapidly to zero.

IV. EXPERIMENTAL CONSEQUENCES

For small r/z_0, the axial motion of a trapped particle (of charge q and mass m) is described by the familiar differential equation of a damped harmonic oscillator:

$$\ddot{z}+\Gamma_z\dot{z}+\omega_z^2 z = F_z/m \ . \tag{4.1}$$

The harmonic-oscillation frequency ω_z is related to the static trapping potentials, of course. The damping constant Γ_z is easily recognized from Eq. (4.1) to be the full width at half maximum of the angular frequency spectrum of the average power dissipated $\langle m\Gamma_z\dot{z}^2\rangle$. The source of the damping will be discussed presently. Static and oscillatory axial forces together comprise F_z.

A small static offset potential $V_{\rm dc}$ as in Eq. (2.1), whether it is due to trap imperfections or is applied deliberately, shifts the center of the axial oscillation from $z=0$ to the equilibrium value $z=z_e$ given by

$$\frac{z_e}{z_0} = -\frac{d^2}{2z_0^2}\frac{qV_{\rm dc}}{m\omega_z^2 d^2}B_1 \ , \tag{4.2}$$

which is obtained by setting the derivatives equal to zero in the differential equation and approximating F_z by its leading term. This expression can be simplified for an asymptotically symmetric trap with hyperbolic electrodes since in this case $d=z_0$ and $m\omega_z^2 d^2 \approx qV_0$, with V_0 being the difference between the endcap and ring potentials in the absence of an offset potential. In this special case, $B_1=0.80$ from Eq. (3.5) so that

$$\frac{z_e}{z_0} \approx -\frac{4}{10}\frac{V_{\rm dc}}{V_0} \ . \tag{4.3}$$

Consider, for example, a potential $V_{\rm dc}=1$ volt applied to the asymptotically symmetric trap of Fig. 1 while an electron is trapped within it. Typically the trapping potential $V_0 \approx 10$ volt so that $z_e/z_0 \approx 4\times 10^{-2}$.

Translating the center of the axial oscillation has proven to be useful in experiments which make use of magnetic bottles (most notably in the recent proton experiments[10]) to measure the size of the magnetic bottle, to determine its precise location with respect to the electric center of the trap, and finally to shift the electric center to coincide with the magnetic center. Until this calculation, the accuracy in the measurement of the size of a magnetic bottle was limited because the value for B_1 was not well known. Thus, the version of Eq. (4.3) contained in Ref. 11 yields z_e/z_0 which differs by 25% because B_1 was approximated by 1. In response to this work, my colleague Van Dyck has interpreted some earlier data for a trapped electron as a measurement of B_1 for an asymptotically symmetric trap with hyperbolic electrodes.[11] The size of the magnetic bottle was measured by observing the axial frequency shift brought about by a spin flip.[3] Static offset potentials were then applied to the endcaps to move the center of the axial oscillation. A shift in the cyclotron frequency was observed as the electron was repositioned in the inhomogeneous field of the magnetic bottle. The resulting experimental value for B_1 agrees with the value from the relaxation calculation in Eq. (3.5) and is plotted with its uncertainty in Fig. 8. Despite the large error bars, this test of the calculated value is important because the measured values of B_1 deduced by a radio-frequency technique (discussed in the following paragraphs) differ substantially from the calculated values. In so far as the above measurement can be done only in a trap with a magnetic bottle and requires the observation of the axial frequency shift which results from a spin flip, it is not a generally available technique.

In the remaining paragraphs of this section we focus upon the oscillatory potentials on the electrodes that are relevant to the axial motion of a trapped particle. To lowest order in r/z_0, ϕ_A is approximated as $B_1 z/2z_0$ so that the oscillatory drive potential V_D and the oscillatory noise potential V_n produce an axial force (in addition to the static force discussed above) given by

$$F_z \approx q\frac{(V_D - V_n)}{2z_0}B_1 \tag{4.4}$$

on a trapped particle of charge q and mass m. To discuss the damping constant Γ_z to first order in r/z_0, however, we take advantage of the fact that the differential equation (4.1) is linear and we thus consider the special case of $V_n=V_D=0$. We thus assume that Γ_z is independent of both of these drives and our discussion initially parallels the earlier discussion of Wineland and Dehmelt.[9] The damping of the axial oscillation is due to the power (V_I^2/R) dissipated in the resistor R as originally discussed by Dehmelt and Walls.[15] This dissipated power is also what is detected. Radiative damping also occurs but is negligibly small because ω_z is a radio frequency. Equating the rate that the particle does work on the induced fields within the trap (given by $qV_I\dot{z}\partial\phi_A/\partial z$) to the power dissipated in the resistor in the limit of small r/z_0 yields

$$V_I \approx \frac{qB_1}{2z_0}R\dot{z} \ . \tag{4.5}$$

The amplifiers (in Fig. 4) are sensitive to V_I+V_n with V_I the desired signal and V_n a major part of the undesirable noise. Since $V_n^2 \propto R$, the ratio of the powers $V_I^2/V_n^2 \propto R$ so that R is typically made as large as possible.

The damping width Γ_z is also proportional to R. The induced potential V_I produces a repulsive force on the trapped particle, $-qV_I\partial\phi_A/\partial z$. In the limit of small r/z_0, Eq. (4.5) can be used to write this dissipative force

in the conventional way as $-m\Gamma_z\dot{z}$ with

$$\Gamma_z=\frac{1}{m}\left[\frac{qB_1}{2z_0}\right]^2 R\ . \tag{4.6}$$

Small changes in B_1 thus produce bigger changes in Γ_z.

For convenient analysis of detection electronics, Wineland and Dehmelt[9] showed that the above discussion can be formulated in terms of an equivalent series *lc* circuit which represents the trapped particle and is connected between the endcaps as indicated by dashed symbols in Fig. 4. The *lc* circuit is resonant at ω_z (so that $\omega_z^2=1/lc$) and $l=R/\Gamma_z$. This model emphasizes that on resonance a trapped particle acts like a short circuit so that $V_I+V_n=V_D$. Part of the induced potential V_I cancels the thermal noise potential V_n exactly on resonance. In practice, hopes for extremely high enhancements of the signal to noise ratio on resonance[16] have not yet been realized primarily because trap anharmonicities and trapping potential fluctuations introduce an effective spread in the resonance frequency ω_z.

The above discussion for small r/z_0 can also be extended to the center-of-mass motion of a cloud of N trapped particles[9] which acts much like the motion of a particle of charge Nq and mass Nm. Both ω_z and F_z/m are independent of N since they are functions of only the charge-to-mass ratio. The effective damping width for the center-of-mass motion of N particles, however, is given by

$$\Gamma_N=N\Gamma_z \tag{4.7}$$

since the damping constant goes as the charge squared over the mass. Differential equation (4.1) thus applies to the center-of-mass motion of a cloud of N charged particles when Γ_z is replaced by Γ_N. Measurements of the axial linewidth Γ_N have thus been used to determine N, most recently in the experiment to measure the ratio of the electron and proton masses, since a single proton has not yet been trapped.[6] A series *lc* circuit model also applies for N particles with $l_N=l/N$ and l_Nc_N resonant at ω_z.

The analysis of axial detection and damping for small r/z_0 requires the numerical value of only the constant B_1. Dehmelt and Walls[15] estimated that $B_1\approx 0.9$, whereas Wineland and Dehmelt[9] estimated that $B_1\approx\frac{1}{2}$. Although these estimates were never taken very seriously for their own sakes, a measured value of $B_1\approx\frac{1}{2}$ for electrons and positrons in the asymptotically symmetric trap of Fig. 1 and several others was taken much more seriously.[17] After a single particle was unambiguously trapped, and the anharmonicity tuned out of the trap, the value of $(B_1)^2$ was deduced from the measured value of Γ_z using Eq. (4.6). The present relaxation calculation was then undertaken to check for departures from the measured value of B_1 for different ρ_0/z_0, r_c/z_0, and α. Instead, the calculated value of Γ_z/R unexpectedly turned out to be larger than the measured value by more than a factor of 2. For a given R, the measured axial widths are thus narrower than predicted by the relaxation calculation value of B_1 and Eq. (4.6) by this factor.

One possible source of the discrepancy is higher-order terms in the expansion of the potential. These can be readily examined because the relaxation calculation produces B_3. Terms through the B_3 term can be accounted for in the formulas of this section if B_1 is replaced by

$$B_1'=B_1+\frac{2z/z_0}{1+\rho_0^2/2z_0^2}+3B_3\frac{z^2-\rho^2/2}{z_0^2}\ . \tag{4.8}$$

The second term comes from the quadrupole potential in Eq. (2.4) and thus is only present for the detection configuration of Fig. 4(b) and not for that of Fig. 4(a). Including these terms provides a much improved approximation because the relaxation calculation shows that higher-order B_k are negligible for $\rho<\rho_0$, especially for asymptotically symmetric traps.

The substitution (4.8) should properly be used to derive a more complicated differential equation to replace Eq. (4.1). We take instead a more qualitative approach. Recall that $\Gamma_z\propto(B_1)^2$ in Eq. (4.6) and thus note that only the $-\rho^2/2$ term in the substitution (4.8) is capable of reducing Γ_z. If we focus on this term and neglect the others we find that Γ_z gets replaced by Γ_z' which depends upon ρ^2 by

$$\Gamma_z'=\Gamma_z\left[1-\frac{6B_3}{B_1}\frac{\rho^2}{2z_0^2}\right]\ . \tag{4.9}$$

This approximation is not as arbitrary as it may first seem. The terms neglected all go as some power of z/z_0. There is every reason to believe that these terms are relatively small because the axial motion is naturally damped as described above. The magnetron motion of a trapped particle, however, is essentially decoupled from its environment so that rather large values of ρ are possible. For an asymptotically symmetric trap $\rho^2/2z_0^2$ is equal to $(\rho/\rho_0)^2$ and a realizable magnetron radius of $\rho/\rho_0\approx 0.6$, in fact, would make Γ_z' approximately equal to the axial width observed in asymptotically symmetric traps. The problem with this scenario is that electrons are typically loaded near the z axis where $\rho/\rho_0<10^{-2}$ and sideband cooling has been carefully used to reduce ρ below this value, to $\rho/\rho_0\approx 3\times 10^{-3}$ according to Ref. 3. Higher-order terms are thus not able to explain the discrepancy between the measured and calculated values of Γ_z.

A more likely source for the disagreement between measured and calculated Γ_z/R is difficulties in measuring R and/or Γ_z. A consistent mismeasurement of R by more than a factor of 2 is difficult to imagine, however. The measurement of Γ_z is generally open to some misinterpretation because of electrostatic anharmonicity, but anharmonicity can only broaden (not narrow) the observed resonance width. Electrical feedback from the output of the amplifier to the drive endcap [the lower endcap in Fig. 4(b)] could effectively reduce R in the desired manner. It seems unlikely, however, that such feedback should be so uniformly present in different experimental arrangements.[16] Deliberate attempts to produce such feedback revealed that it was not easily established.[18] No convincing explanation of the discrepancy has thus yet emerged.

ACKNOWLEDGMENTS

I am thankful to Lowell Brown, Hans Dehmelt, Paul Schwinberg, and Phil Ekstrom for helpful conversations

and comments on the manuscript. I am also grateful to Robert Van Dyck for the measured value of B_1 that he provided (along with helpful comments) as a check on this work, to Fred MacKintosh for adapting the conformal mapping solution, and to Jim Pickrell for the electrolytic tank measurement. This work was supported by the National Science Foundation.

---

[1]D. Wineland, P. Ekstrom, and H. Dehmelt, Phys. Rev. Lett. 31, 1279 (1973).

[2]Reviewed in H. Dehmelt, *1982/83 McGraw-Hill Yearbook of Science and Technology* (McGraw-Hill, New York, 1982); P. Ekstrom and D. Wineland, Sci. Am. 243, 105 (1980).

[3]R. S. Van Dyck, Jr., P. B. Schwinberg, and H. Dehmelt, in *New Frontiers in High Energy Physics,* edited by B. Kursuhoglu, A. Perlmutter, and L. Scott (Plenum, New York, 1978); Bull. Am. Phys. Soc. 24, 758 (1979).

[4]P. B. Schwinberg, R. S. Van Dyck, Jr., and H. G. Dehmelt, Phys. Rev. Lett. 47, 1679 (1981).

[5]T. Kinoshita and W. B. Lindquist, Phys. Rev. Lett. 47, 1573 (1981).

[6]R. S. Van Dyck, Jr., and P. B. Schwinberg, Phys. Rev. Lett. 47, 396 (1981); R. S. Van Dyck, Jr., F. L. Moore and P. B. Schwinberg, Bull. Am. Phys. Soc. 28, 791 (1983).

[7]G. Gabrielse and H. Dehmelt, in *Precision Measurements and Fundamental Constants II,* edited by B. N. Taylor and W. D. Phillips, Natl. Bur. of Standards (U.S.), Spec. Publ. 617, 1981 (in press).

[8]G. Gabrielse, Phys. Rev. A 27, 2277 (1983).

[9]D. Wineland and H. Dehmelt, J. Appl. Phys. 46, 919 (1975).

[10]R. S. Van Dyck, Jr., P. B. Schwinberg, and S. B. Bailey, in *Atomic Masses and Fundamental Constants 6,* edited by J. A. Nolen, Jr. and Walter Benenson (Plenum, New York, 1980).

[11]R. S. Van Dyck interpreted some data taken earlier as a measurement of B_1 in order to test this calculation.

[12]F. Walls, Ph. D. thesis (unpublished).

[13]G. Gabrielse and F. MacKintosh, Int. J. Mass. Spectrosc. Ion Phys. (to be published).

[14]The conformal-mapping solution was adapted by Fred MacKintosh from P. Henrici, *Applied and Computational Complex Analysis* (Wiley, New York), Vol. 1, pp. 343–345.

[15]H. G. Dehmelt and F. L. Walls, Phys. Rev. Lett. 21, 127 (1968).

[16]H. Dehmelt, P. Ekstrom, and D. Wineland, Bull. Am. Phys. Soc. 19, 572 (1974).

[17]The measurements in the trap of Fig. 1 were by the author. Measurements in the electron trap of Ref. 3 and with electrons trapped in the proton trap of Ref. 6 were by R. S. Van Dyck.

[18]R. S. Van Dyck, private communication.